Available online at www.sciencedirect.com
SCIENCE DIRECT®
Chemical Physics Letters 378 (2003) 368–373
CHEMICAL PHYSICS LETTERS
www.elsevier.com/locate/cplett

# Spontaneous growth and luminescence of Si/$SiO_x$ core-shell nanowires

Changfeng Wu [a,b,*], Weiping Qin [a,b,*], Guanshi Qin [a,b], Dan Zhao [a,b], Jisen Zhang [a,b], Wu Xu [a,b], Haiyan Lin [a]

[a] *Key Laboratory of Excited State Processes, Chinese Academy of Sciences, Changchun 130033, PR China*
[b] *Changchun Institute of Optics, Fine Mechanics and Physics, Chinese Academy of Sciences, Changchun 130022, PR China*

Received 22 May 2003; in final form 26 June 2003
Published online: 26 August 2003

**Abstract**

Silicon nanowires were prepared by a thermal evaporation of $MoSi_2$ heating rods under controlled temperature and atmosphere. Transmission electron microscopy and selected area electron diffraction show that the nanowire consists of a crystalline Si core and an amorphous $SiO_x$ shell. There exist two major forms of nanowires possessing different morphologies and growth directions, which may indicate that different mechanisms predominate in the growth process. The photoluminescence of the Si/$SiO_x$ core-shell nanowires presents two emission bands, around 550 and 600 nm, respectively.


## 1. Introduction

One-dimensional (1D) nanoscale structures have attracted a great deal of attention in recent years because of their great potential for fundamental studies as well as applications in functional nanodevices [1,2]. Various 1D nanostructures such as nanowires [3], nanocables [4], nanobelts [5], nanotubes and nanofiber arrays [6] have been demonstrated recently. Particularly, silicon nanowires are very attractive due to the central role of Si in the semiconductor industry and its mature fabrication technology. The synthesis of crystalline Si nanowires holds considerable technological promise for semiconductor nanodevices such as nanowire p–n junctions and field-effect transistors [7–9]. Many successful strategies have been developed for Si nanowire fabrication. Morales and Lieber [10] have extrapolated on the ideas entailed in the vapor–liquid–solid (VLS) technique to develop the laser ablation metal–catalytic method for the synthesis of crystalline Si nanowires. Lee and coworkers [11] have demonstrated the oxide-assisted catalyst-free method as a means of obtaining bulk quantities of Si nanowires. However, the

* Corresponding authors. Fax: +864314627031.
*E-mail addresses:* chfwumail@yahoo.com (C. Wu), wpqin@public.cc.jl.cn (W. Qin).

0009-2614/$ - see front matter © 2003 Elsevier B.V. All rights reserved.
doi:10.1016/j.cplett.2003.08.005

nanowires prepared by this method generally display twinnings, high order grain boundaries, and stacking faults. Gole et al. [12] have modified this approach by elevated temperature synthesis and generated virtually defect-free crystalline Si nanowires. Since material properties strongly depend on dimensionality and crystallinity, great effort has been made to control the sizes, morphologies, and lattice orientations of silicon nanowires in order to tune their electrical or optical properties.

In this Letter, we report the synthesis and luminescence of Si nanowires obtained by a simple thermal evaporation of molybdenum disilicide ($MoSi_2$) heating rods. Each nanowires consists of a single crystalline core covered by an amorphous oxide sheath. Although they were obtained under the same conditions, the nanowire long axes occur along different lattice orientations, which suggests that different mechanisms predominate in the growth process. The photoluminescence (PL) properties were discussed.

## 2. Experimental

Our synthesis is based on thermal evaporation of $MoSi_2$ rods under controlled temperature and atmosphere. The apparatus for these experiments has been used to prepare an ordered $Si_{1-x}C_x$ alloy, as described in our recent report [13]. Fig. 1 shows the schematic diagram of the high-temperature oven system. A muffle furnace equipped with $MoSi_2$ rods was used as the heating device. The pressure in the inner furnace was under a normal atmospheric pressure in air. A 20 ml alumina crucible filled with ammonium hydrogen difluoride ($NH_4F \cdot HF$) was placed at the center of the furnace where the temperature was kept at 900 °C. At this temperature, $NH_4F \cdot HF$ was decomposed into $N_2$, $H_2$, and HF gases, the two active components of which generated a reducing atmosphere in the furnace, resulting in the evaporation of the $MoSi_2$ heating rods. The system was held at this temperature for 2 h. After it had cooled to room temperature, the gray products were collected from the surfaces of $MoSi_2$ rods.

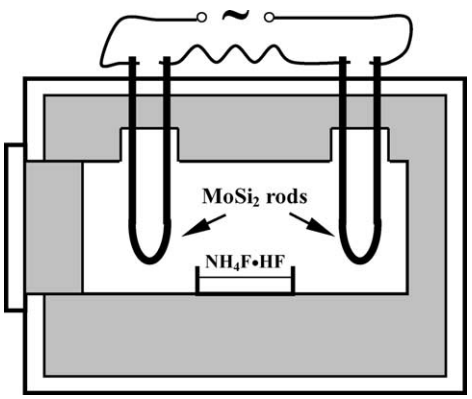


Fig. 1. Schematic diagram of the Muffle furnace used for the synthesis of crystalline Si nanowires.

The general morphology and chemical composition of the products were characterized by scanning electron microscope (SEM, KYKY 1000B) equipped with energy-dispersive X-ray spectroscopy (EDX), and X-ray photoelectron spectroscopy (XPS, VG Escalab MK Π). Detailed structure analysis was carried out by transmission electron microscope (TEM, JEOL 2010) operating at 200 kV. The specimens for SEM observations were supported by aluminum substrate, and those for TEM investigations were placed on holey copper grid with carbon film. With the excitation of a 488 nm $Ar^+$ laser, PL spectrum was measured by a Jobin-Yvon 630 micro-Raman system at room temperature.

## 3. Results and discussions

Fig. 2a shows a typical SEM image of the synthesized material. The products possess a wire-like morphology. The nanowires appear to be relatively uniform, with an average diameter of ~100 nm, and length up to several micrometers. Those displaying larger diameters are bundle aggregates of several nanowires in which a single nanowire cannot be clearly distinguished due to the low resolution of the SEM. The EDX analysis, as illustrated in Fig. 2b, reveals that the sample contains Si in abundance with the presence of oxygen and a trace Mo element. The Al peaks were generated from the supporting Al substrate. The composition of the sample was further determined

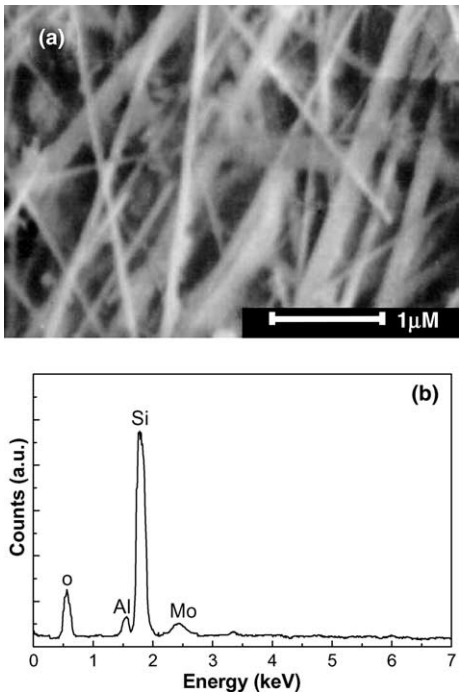


Fig. 2. (a) SEM image of the as-prepared nanowires. (b) EDX spectrum of the products.

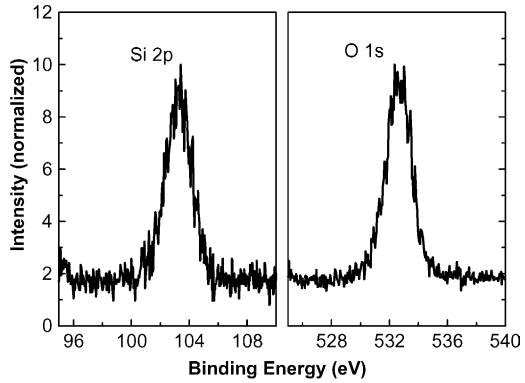


Fig. 3. Silicon (2p) and oxygen (1s) electron spectra for the Si/$SiO_x$ nanowires.

by XPS measurements. According to the XPS data in Fig. 3, the element ratio of Si:O was calculated to be 58:42, while no Al and Mo element were detected. Since XPS technique is confined to surface analysis, the measured value may be a representative composition for the surface sheath of the nanowires.

The morphology and structure of the as-prepared products have been characterized in detail using TEM and selected area electron diffraction (SAED). Two major forms of silicon nanowires are observed from the TEM images in Fig. 4. Nanowires with rough surfaces and twisted shapes are one representative component (marked as Sample A, indicated in Fig. 4a), while the other kind show smooth surfaces and straight shapes (marked as Sample D, indicated in Fig. 4d). In addition, Si nanoparticles (minor component in the products) are found to coexist with the nanowires, and some of them self-assemble together and appear in the form of short chain. Further magnified TEM images and SAED on individual nanowires provide further insight into the structure of these materials, as illustrated in Figs. 4c,e which correspond to Samples A and D, respectively. In Fig. 4c, a light/dark/light contrast is observed along the radial direction of the nanowire, suggesting a different phase composition between the central part and the two peripheries of the nanowire, which leads to the coaxial core-shell structure. TEM observation of several tens of such nanowires reveal that the diameter of the core and the thickness of the shell are relatively uniform, in the range of 20–30 nm. The inset shows the SAED pattern recorded perpendicular to the nanowire long axis, which could be indexed for the [1 1 0] zone axis of single crystalline Si and suggests that the nanowire growth occurs along the $[1\,\bar{1}\,2]$ direction. Since only one set of diffraction spots corresponding to the core can be observed, together with the XPS data, it is inferred that the shell is composed of amorphous silicon oxide. In regard to Sample D, a typical image of a nanowire tip is shown in Fig. 4e. The amorphous $SiO_x$ shell appears darker than the crystalline Si core in this imaging mode. Particularly, the shell becomes thinner and thinner when approaching the tip of the nanowire, and eventually only the core is maintained. The SAED pattern (Fig. 4e, inset) is taken from the single core at the tip area. It could be indexed for the [2 1 1] zone axis of single crystalline Si, and indicates that the nanowire growth occurs along [1 1 1] direction. A typical TEM image of a Si nanoparticle chain is presented in

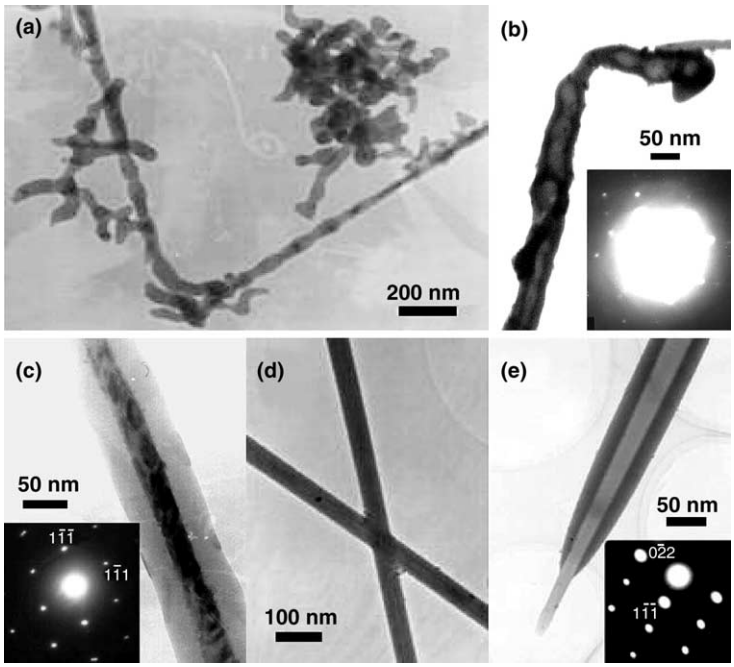


Fig. 4. (a) TEM morphology of the Si nanoparticle chains and Sample A showing twisted shapes and rough surfaces. (b) Magnified TEM image and SAED pattern for the Si nanoparticle chain. (c) Magnified TEM image and SAED pattern for Sample A. (d) TEM morphology of Sample D showing straight shapes and smooth surfaces. (e) Magnified TEM image and SAED pattern for Sample D.

Fig. 4b. Actually, the trunk of the chain looks more like a nanowire, while there still have several discrete Si particles clad by thick $SiO_x$ shell near the end. The inset gives the SAED pattern taken from the end of the chain. Obviously, the pattern does not originate from a single crystal. Some weak diffraction spots are outlined irregularly, which means that the nanoparticles in the chain have different crystalline orientations.

Several models have been proposed to explain the growth of crystalline Si nanowires including the VLS mechanism [10] and the oxide-assisted method [11]. The main characteristic of the VLS mechanism is the presence of liquid intermediates that serve as catalysts between the vapor precursors and the solid products. Accordingly, the morphology is featured by a catalyst particle located at the end of the nanowire. Although the metal element (Mo) was contained in the starting materials and also detected in the products, the Mo element seems not to serve as a catalyst for VLS growth because the molybdenum disilicide has so high a melting point (2030 °C) that it cannot form liquid droplets at the growth temperature. Experimentally, no nanoparticles were observed on any end of the Si nanowires, so the VLS mechanism cannot explain the growth of the Si nanowires. Since the nanowires were grown on the $MoSi_2$ rods, it is unavoidable that the trace Mo component was contained in the products, as indicated by EDX measurements. The XPS results demonstrate that it is not at the surface of the wire. Presumably, the trace Mo component may be embedded in the amorphous $SiO_x$ shell. However, detailed SAED experiments on individual nanowires cannot find any information regarding the Mo element due to its low concentration.

Two major forms of Si nanowires coexist in the products, which suggests that there may exist two possible mechanisms predominating the growth process. The oxide-assisted process is likely to operate in the growth of Sample A, since our synthesis can meet all the growth conditions for this mechanism. In the experiment, the $MoSi_2$ rods

serve as the heating element. Generally, on the surfaces of the $MoSi_2$ rods there form protective layers composed of $SiO_2$, which resist the oxidation of the heating rods at elevated temperature. The two active gases, HF and $H_2$, originating from the decomposition of $NH_4F \cdot HF$, can deoxidize $SiO_2$, and some silicon seeds nucleate from silicon oxide at this stage. The silicon seeds would serve as the nuclei for the growth of Si nanowires in the oxide-assisted process, as described in detail by Lee and co-authors [11,14,15]. A number of factors have been proposed to determine the growth kinetics. For example, the $Si_xO$ ($x > 1$) layer at the tip of each nanowire seems to act as a catalyst. The $SiO_2$ shell might help to retard the lateral growth of each wire. The presence of a $\{1\,1\,1\}$ surface parallel to the axes of the nanowires can minimize the system energy, since the $\{1\,1\,1\}$ surface has the lowest surface energy among the Si surfaces, which becomes increasingly important when the crystal size is largely reduced to nanometer scale. These important factors may determine the growth direction of Si nanowires to be $\langle 1\,1\,2\rangle$. The oxide-assisted mechanism can predict some of the morphology of nanowires [11], which were entirely observed in Fig. 4. For example, Si nanoparticles coexist with the nanowires and some nanoparticles with different orientations self-organize into the form of short chains. The nanowires exhibit rough surfaces and twisted shapes. Particularly, the nanowire growth occurs along the $\langle 1\,1\,2\rangle$ direction. These features suggest that the growth of Sample A follows the oxide-assisted mechanism. However, this mechanism seems not suitable to account for the growth of Sample D, since the morphology and growth direction are not compatible with the results observed in the oxide-assisted process. Gole et al. [12] have demonstrated that virtually defect-free silica sheathed Si nanowires growing in the $\langle 1\,1\,1\rangle$ direction can be obtained though a modified approach. In view of the remarkable similarity between our results and their work, the formation of Sample D may follow the mechanisms proposed by Gole et al. which are analogs not only of the VLS mechanism but also represent some crystalline silicon self-assembly.

Under the 488 nm excitation of an $Ar^+$ laser, the PL of the $Si/SiO_x$ nanowires corresponds to two emission bands around 550 and 600 nm, as indicated in Fig. 5a. Each nanowire consists of a crystalline Si core and an amorphous $SiO_x$ shell. The core and shell both can make contributions to the luminescence, as mentioned in early reports [11,16]. In the present case, we propose that the Si core is responsible for the PL band around 600 nm while the other peak originates from the amorphous $SiO_x$ shell. This suggestion is supported by the PL properties of the nanowires annealed at 800 °C for 2 h in an air atmosphere. After the annealing treatment, part of the Si core would be oxidized into the $SiO_x$ shell. Accordingly, the relative luminescence intensity corresponding to the two components would change. Fig. 5b shows the emission spectrum of the as-annealed $Si/SiO_x$ nanowires, which indicates that the PL intensity ratio of 550 nm band to 600 nm band increases compared with that of the sample without annealing. The peak positions of the two spectra remain unchanged, suggesting that no other luminescent species were generated in the annealing process.

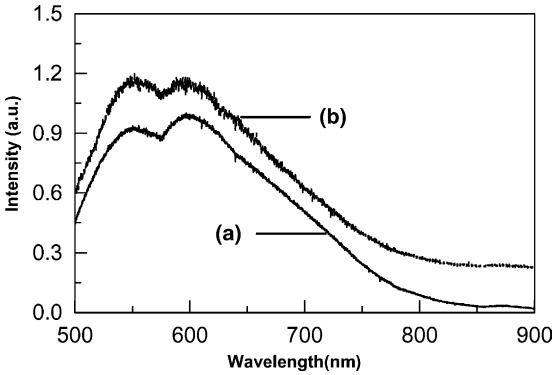


Fig. 5. Photoluminescence spectra for the core-shell $Si/SiO_x$ nanowires (a) before annealing and (b) after annealing.

## 4. Conclusions

Core-shell $Si/SiO_x$ nanowires were prepared by a thermal evaporation of $MoSi_2$ rods in the presence of oxidizing agents under controlled temperature and atmosphere. Two major forms of silicon nanowires are observed from the TEM image. One

with the long axis occurring along ⟨1 1 2⟩ direction may be grown by the oxide-assisted process, while the growth mechanism of the other cannot be definitely determined. The PL of the nanowires corresponds to two emission bands which may originate from the crystalline Si core and the amorphous $SiO_x$ shell, respectively.

## Acknowledgements

This work was supported by the Provincial Natural Science Foundation of Jilin (Grant No. 19990514), the National Natural Science Foundation of China (Grant No. 10274082) and the State Key Project of Fundamental Research of China (Grant No. 1998061309).

## References

[1] Y. Xia, P. Yang, Y. Sun, Y. Wu, B. Mayer, B. Gates, Y. Yin, F. Kim, H. Yan, Adv. Mater. 15 (2003) 353.
[2] Z.W. Pan, Z.R. Dai, Z.L. Wang, Science 291 (2001) 1947.
[3] X.F. Duan, C.M. Lieber, Adv. Mater. 12 (2000) 298.
[4] Q. Li, C. Wang, Appl. Phys. Lett. 82 (2003) 1398.
[5] Y. Zhu, Y. Bando, D. Xue, Appl. Phys. Lett. 82 (2003) 1769.
[6] Z.L. Wang, R.P. Gao, J.L. Gole, J.D. Stout, Adv. Mater. 12 (2000) 1938.
[7] L.J. Lauhon, M.S. Gudiksen, D. Wang, C.M. Lieber, Nature 420 (2002) 57.
[8] Y. Cui, C.M. Lieber, Science 291 (2001) 851.
[9] Z.L. Wang, Z.R. Dai, R.P. Gao, Z.J. Bai, J.L. Gole, Appl. Phys. Lett. 77 (2000) 3349.
[10] A.M. Morales, C.M. Lieber, Science 279 (1998) 208.
[11] N. Wang, Y.H. Tang, Y.F. Zhang, C.S. Lee, I. Bello, S.T. Lee, Chem. Phys. Lett. 299 (1999) 237.
[12] J.L. Gole, J.D. Stout, W.L. Rauch, Z.L. Wang, Appl. Phys. Lett. 76 (2000) 2346.
[13] W. Qin, C. Wu, G. Qin, J. Zhang, D. Zhao, Phys. Rev. Lett. 90 (2003) 245503.
[14] N. Wang, Y.H. Tang, Y.F. Zhang, C.S. Lee, S.T. Lee, Phys. Rev. B 58 (1998) R16024.
[15] W.S. Shi, H.Y. Peng, Y.F. Zheng, N. Wang, N.G. Shang, Z.W. Pan, C.S. Lee, S.T. Lee, Adv. Mater. 12 (2000) 1343.
[16] X.T. Zhou, R.Q. Zhang, H.Y. Peng, N.G. Shang, N. Wang, I. Bello, C.S. Lee, S.T. Lee, Chem. Phys. Lett. 332 (2000) 215.